Journal of Colloid and Interface Science 533 (2019) 207–215

Contents lists available at ScienceDirect

Journal of Colloid and Interface Science

journal homepage: www.elsevier.com/locate/jcis

Regular Article

An entrapped metal-organic framework system for controlled release of ethylene

Yongguang Guan [a,b], Zi Teng [a,b], Lei Mei [b], Jinglin Zhang [b], Qin Wang [b], Yaguang Luo [a,*]

[a] Food Quality Laboratory, United States Department of Agriculture, Agricultural Research Service, Beltsville, MD 20705, USA
[b] Department of Nutrition and Food Science, University of Maryland, College Park, MD 20742, USA

GRAPHICAL ABSTRACT

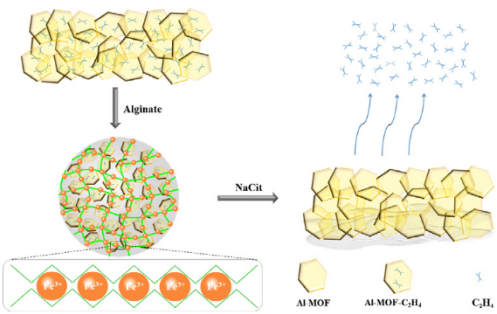

ARTICLE INFO

Article history:
Received 7 July 2018
Revised 19 August 2018
Accepted 20 August 2018
Available online 21 August 2018

Keywords:
Metal-organic framework
Ethylene
Alginate
Sodium citrate
Controlled release

ABSTRACT

A novel gas storage and release system was developed for ethylene, an exogenous plant hormone that regulates fruit ripening and senescence. This system consists of a metal organic framework (MOF) core and an alginate-based shell. The MOF comprises a coordination complex of Al and $[btc]^{3-}$ ligands, which formed hexagonal structure ($P6_3/mmc$) with unit cell of $14.28 \times 14.28 \times 31.32$ Å^3, as revealed by the X-ray diffraction analysis. Ethylene absorption isotherm exhibited an absorption capacity of 41.0 cm^3/g MOF at 25 °C and 101.3 kPa. After charging with ethylene, the MOFs are further entrapped in a close-knit bead formed with alginate-Fe(III) matrix, observed under a scanning electron microscopy coupled with energy dispersive spectroscopy (SEM-EDS). The alginate shell is degraded by exposing to 200 mM sodium citrate aqueous solution, triggering a continuous release of ethylene. With 20 mg of MOF, ethylene concentration reached 0.41–0.46 mg/L per mg MOF after 2.5 h. This is the first report regarding a controlled release of ethylene through degrading alginate-Fe(III) matrix rather than by changing the interfacial pore size of MOF under extreme conditions. This technology can enable precisely controlled and targeted applications of ethylene for food processing and agricultural applications.

Published by Elsevier Inc.

Abbreviations: Al-MOF, aluminum MOF; ANOVA, analysis of variance; CuTPA, copper terephthalate MOF; HF, hydrofluoric acid; ICDD, inductively coupled plasma optical emission; ICP-OES, International Center for Diffraction Data Spectrometry; Me3btc, trimethyl 1,3,5-benzenetricarboxylate; mM, mmol/L; MOFs, metal-organic frameworks; NaCit, sodium citrate; SA, sodium alginate; SD, standard deviation; SEM-EDS, scanning electron microscope-energy disperse spectroscopy; SPSS, statistical product and service solutions; TEOS, tetraethyl orthosilicate; XRD, X-ray diffraction analysis.

* Corresponding author at: Research Food Technologist, Food Quality Lab, Agricultural Research Service, United States Department of Agriculture, Building 002 BARC-West, Room 12, 10300 Baltimore Avenue, Beltsville, MD 20705, USA.

E-mail address: yaguang.luo@ars.usda.gov (Y. Luo).

https://doi.org/10.1016/j.jcis.2018.08.057
0021-9797/Published by Elsevier Inc.

1. Introduction

Storage and controlled release of functional gases are important for the laboratory-, industrial-, and household-scaled applications, such as storage of hydrogen and methane for clean energy applications [1], release of ethylene for fruit ripening [2], etc. Porous materials with large internal surface areas are capable of storing gases [3,4], which are expected for controlled release for practical applications.

Metal-organic frameworks (MOFs) are a class of solid materials consisting of metal ions linked to organic ligands to form one-, two-, or three-dimensional coordination complexes [5–8]. MOFs have ultra-high porosities [9,10], large internal surface areas [11], and tunable cavities [12,13], and have been successfully applied in gas absorption and storage to address various industrial challenges related to energy [6], environment [14], and biological technology [15,16]. A wide variety of MOFs have been used as powerful catalyzing agents [17,18], including palladium-grafted copper-MOF for Suzuki cross-coupling reaction [19], zeolitic imidazolate zinc-MOF for N-formylation [20], and MIL-100(Cr) for selective thioether oxidation [21]. Corma and co-workers summarized the synthesis, structure, and application of MOFs, and suggested that metal sites of MOFs act as both structural building components and coordinate bonding sites, and that the three-dimensional structure built by metal sites and organic ligands generated nanometric cavities as a result of host molecule channels [17]. Recently, a new concept, MOFs for controlled release of loaded substances has garnered significant interests [22–24]. Using heat, redox potential, pH, or light as a promoter, the MOFs enable the controlled release of functional chemicals from the MOF systems at desired time and conditions [25]. However, to the best of our knowledge, a packaging system that can stabilize gas (such as ethylene) encapsulation in MOFs for controlled release has yet to be developed.

Sodium alginate (SA) is a natural polysaccharide obtained from brown seaweeds and certain bacteria [26]. Chemically, SA is a (1-4)-linked block copolymer of β-D-mannuronate and α-L-guluronate with residues arranged in homopolymeric sequences [27,28]. Structural studies have suggested that multivalent ions such as Ca^{2+} and Fe^{3+} can induce SA hydrogel solidification via chain-chain association and form the known egg-box model [29], which is an effective means to close SA gel interfacial pores especially after drying. Additionally, in the presence of ion chelating agents such as citrate and phosphate in aqueous solution, the coordinative multivalent ions can be dissociated from the SA-ion composites [30,31], thus degrading the egg-box structure. Therefore, in this study, the SA-ion composite is used to fabricate an entrapped package system with controlled exposure and release of MOF-loaded substances.

Ethylene is a basic gaseous chemical that has been applied in organic chemical industry [32–34], biological medicine [35], and food processing and preservation [36,37]. Ethylene cluster with a carbon-carbon double bond structure promotes the intermolecular adsorption with electron acceptors [38], such as coordinating with unsaturated metal ion sites. Meanwhile, the CH-π interaction has been determined between ethylene cluster and benzene ligand [38]. Therefore, there is a possibility that ethylene molecules may have an interaction with the porous MOF interface both on the sites of metal ion nodes and organic ligand linkers. Recent studies have offered new insight into loading ethylene into MOFs, as novel ethylene carriers [2,39–42] with potential applications in catalysis, gas separation, and fruit ripening. However, in consideration of practical applications, much work is needed to develop an appropriate packaging system that can stabilize ethylene encapsulation in MOFs and allow application of ethylene at will by consumers rather than immediately after loading into MOFs.

The main objective of this study is to develop an aluminum metal-organic-framework (Al-MOF) packaging system for ethylene storage and controlled release using sodium citrate (NaCit) solution as a promoter (Scheme 1). The physicochemical properties of the developed ethylene-Al-MOF packaging system, including interfacial properties, chemical composition, and dynamic release of ethylene are also studied. Although there are a few researchers reporting the controlled release of MOF-loaded substances using electricity [22] and acid [23] as promoters, sodium citrate is a milder means that may be more suitable for releasing ethylene, which is flammable, from the interfacial pores of MOFs, especially for consumer applications. In addition, the existing switchable MOFs in recent reports [22–24] focused on the change of interfacial pores affected by the promoters, which is very different compared to our MOF packaging system using "encapsulation" concept without changing the MOF interfacial pores.

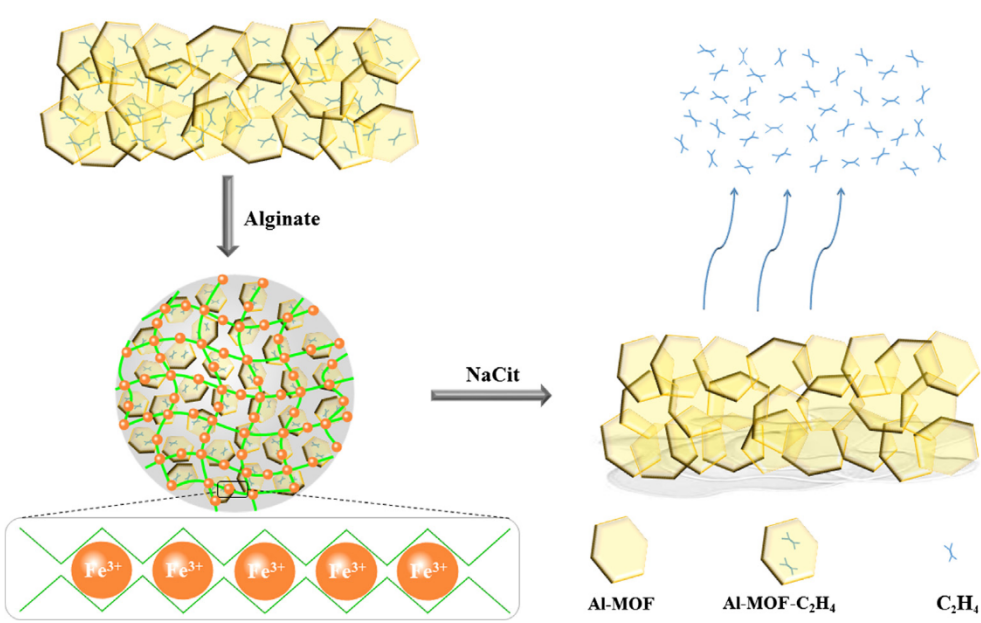

Scheme 1. Illustration of the NaCit-induced Al-MOF exposure for controlled release of ethylene.

2. Materials and methods

2.1. Chemicals

Aluminum nitrate nonahydrate ($Al(NO_3)_3 \cdot 9H_2O$) (purity ≥98%), trimethyl 1,3,5-benzenetricarboxylate (Me_3btc) (98%), hydrofluoric acid (HF) 48 wt.% in H_2O (purity ≥99.99%) and tetraethyl orthosilicate (TEOS) (98%) were purchased from the Sigma-Aldrich Corp. (St. Louis, MO, USA). Sodium alginate (TICA-algin 400 powder) was purchased from the TIC Gums, Inc. (Belcamp, MD, USA), sodium citrate (NaCit) dehydrate from the VWR International (West Chester, PA, USA), and ferrous sulfate heptahydrate ($FeSO_4 \cdot 7H_2O$) and ferric chloride hexahydrate ($FeCl_3 \cdot 6H_2O$) from the Mallinckrodt Baker, Lnc. (Phillipsburg, NJ, USA). The ethylene and air at purity higher than 99% were purchased from the Airgas Inc. (Gaithersburg, MD, USA). Deionized water (DI-water) with a resistivity higher than 18 MΩ cm (Millipore SUPER-Q, Darmstadt, Germany) was used in this study.

2.2. Al-MOF synthesis

Al-MOF was synthesized according to a modified method [43]. Briefly, 1.183 g $Al(NO_3)_3 \cdot 9H_2O$ was dissolved in 18 mL water with subsequent addition of 0.54 mL of 4.8% hydrofluoric acid (HF), 0.396 g Me_3btc and 0.144 mL tetraethyl orthosilicate (TEOS). The mixture was tightly sealed and incubated in a teflon-lined steel Parr autoclave at 210 °C for 24 h. After the hydrothermal reaction, a powdered product was obtained, which was filtered, washed 3 times with 100 mL DI-water, and vacuum dried for ~16 h to obtain the Al-MOF. The HF and TEOS were used for their mineralizing effect in reaction, which promote the crystal growth and increase the crystallinity degree.

2.3. Al-MOF@alginate-Fe(III) beads synthesis

Briefly, 50 mg SA was dispersed in 2.5 mL DI-water and hydrated at 21 °C overnight. Then, 50 mg Al-MOF (mass ratio of Al-MOF to SA = 1:1) was added into the SA dispersion with thorough stirring. The Al-MOF suspension was subsequently introduced into 200 mM $FeCl_3$ solution using a Chemyx Fusion 720 Touch syringe pump (Chemyx Inc., Stafford, TX, USA) to fabricate beads. After 30 min solidification, beads were filtered and washed 3 times with DI-water to remove free Fe(III) that was physically adsorbed on the surface of beads. The clean beads were dried under atmospheric condition overnight (~16 h) to obtain Al-MOF@alginate-Fe(III) beads.

2.4. Characteristics

2.4.1. Polarizing microscope observation

Al-MOF powder was dispersed on a glass sheet, and subsequently observed using a Nikon, Eclipse LV100 Pol polarizing microscope (Nikon, Tokyo, Japan). Representative images are shown in Section 3.1.

2.4.2. Transmission electron microscope (TEM)

Two microliters of Al-MOF in aqueous suspension was dropped on a 200-mesh carbon-coated copper grid. The Al-MOF was subsequently air dried overnight at ambient temperature and observed under a Tecnai T12 TEM (FEI Company, Hillsboro, OR, USA) for its crystallinity. Representative images are shown in Section 3.1.

2.4.3. X-ray diffraction analysis (XRD) crystallography

The Al-MOF was dried in vaccum overnight at ambient temperature for XRD analysis. A Bruker D8 Advance powder X-ray diffractometer (Bruker AXS GmbH, Karlsruhe, Germany), equipped with a Cu sealed tube (wavelength 0.154 nm), Ni beta-filter and LynxEye position sensitive detector was used to analyze the Al-MOF. The XRD patterns were obtained at the 2θ angle range of 5–65° at a rate of 0.02° per second for unit cell refinement and crystal cell structure determination. Spectrum analysis and phase identification were performed using the International Center for Diffraction Data (ICDD) powder diffraction database.

2.4.4. Measurement of ethylene adsorption isotherm

The ethylene adsorption isotherm by Al-MOF was determined as reported in our early study [2]. A low-pressure (P < 101.3 kPa) ethylene isotherm was measured using a Micromeritics ASAP unit at 25 °C. The Al-MOF powders were activated on a Smart VacPrep (Micromeritics Instrument Corp., GA, USA) unit by degassing in stages up to 150 °C with a series of ramp/soak steps under dynamic vacuum. The Al-MOF powder was vacuumed while temperature increased from room temperature to 80 °C at 1 °C per min. The temperature was then held at 80 °C for 1 h until a vacuum level of <0.133 Pa was reached, ramped at 10 °C/min to 150 °C for an additional 1 h, and finally held at 150 °C until a vacuum level of <0.0133 Pa was achieved. The ethylene volume absorption by per unit of mass of Al-MOF was determined to understand the ethylene loading capability by Al-MOF powders.

2.4.5. Scanning electron microscope-energy dispersive spectrometer (SEM-EDS)

SEM-EDS (Hitachi SU-70 Pleasanton, CA) was applied to analyze the three-dimensional morphology, elemental composition and distribution of Al-MOF, and the cross section and surface of the Al-MOF@alginate-Fe(III) beads. The Al-MOF@alginate-Fe(III) beads were cut using a razor blade before the SEM-EDS measurement. All samples were coated with a thin layer of gold before SEM-EDS determination against the collapse and surface damage of the electron beam sensitive objective materials [44]. Representative images are shown in Sections 3.1 and 3.3.

2.4.6. Measurement of Fe and Al-MOF

Briefly, 10 mg of SA-Fe(III) beads with or without entrapped Al-MOF were suspended in 10 mL of 200 mM NaCit solution with stirring at 900 rpm overnight to completely collapse the SA-Fe (III) beads and to fully dissolve SA and Fe ion in solution. All samples were centrifuged at 1500g for 10 min, and the supernatant was detected by an ICPE-9000 inductively coupled plasma optical emission spectrometry (ICP-OES, Shimadzu Scientific Instruments (Oceania) Pty Ltd., Rydalmere, New South Wales, Australia) to quantify the dissociated Fe(III) ions. The precipitate was washed 3 times with DI-water and vacuum dried overnight to calculate the Al-MOF loading capability by Eq. (1).

$$\text{Al} - \text{MOF loading capability}(\%) = 100 \times \frac{m}{m_0} \quad (1)$$

where the m is the mass of Al-MOF obtained after beads collapse, and m_0 is the mass of dried Al-MOF@alginate-Fe(III) beads.

2.4.7. Dynamic collapse of Al-MOF@alginate Fe(III) beads

The 10 mg Al-MOF@alginate Fe(III) beads were suspended in 10 mL of 200 mM NaCit solution at ambient temperature for 0, 0.5, 1, 1.5, 2 and 2.5 h. The insoluble alginate was gently removed from the solution using clean forceps. The remaining suspension was centrifuged at 1500g for 10 min. The supernatant was collected in the same manner as above for Fe quantitative analysis by ICPE-9000. The precipitate was washed 3 times with water, and vacuum dried for ~1 day to quantitatively analyze Al-MOF.

2.5. Ethylene loading

Ethylene was loaded according to our earlier protocol [2]. Briefly, 50 mg Al-MOF powder was vacuumed in a desiccator at ambient temperature for 1 h to fully remove air from the chamber. Then, pure ethylene was infused into the desiccator until ambient pressure was reached, and the powder was kept in the chamber for 3 h. Subsequently, the powder was removed and immediately suspended in 2.5 mL 2% (w/w) SA solution in a 20-mL close glass vial. After stirring for 5 min, the suspension was added dropwise into 10 mL of 200 mM $FeCl_3$ solution using a Chemyx Fusion 720 Touch syringe pump (Chemyx Inc., Stafford, TX, USA). The resultant mixture was stirred for ~30 min for bead solidification. The solidified samples were dried overnight in a desiccator containing montmorillonite desiccants and charged with ethylene to prepare dried ethylene loaded Al-MOF@alginate beads.

2.6. Ethylene release measurement

Briefly, 43 mg of dried Al-MOF@alginate-Fe(III) beads, containing 20 mg Al-MOF, charged with ethylene were suspended in 10 mL of 200 mM NaCit solution, which was then transferred to a 20-mL closed vial. After 2.5 h of incubation at room temperature, the vial was opened and immediately transferred to a 4-L close glass container to initiate gas release. All samples were maintained at ambient temperature and pressure. At predetermined intervals, 20 mL samples were drawn from the headspace of glass container with a syringe and injected into an ETD-300 Ethylene Detector (Sensor Sense, Nijmegen, The Netherlands). A glass column containing montmorillonite desiccant was equipped to remove moisture from the gas sample prior to detection. The measurement was conducted with air as the carrier gas, at temperature of 200 °C and flow rate of 5 L/h. The ethylene in the environment was also measured for baseline correction.

2.7. Statistical analysis

The measurement of Al-MOF and Fe contents and dynamic collapse of Al-MOF@alginate Fe(III) beads were carried out in triplicate. Data were analyzed using the PROC MIXED procedure by SAS (ver. 9.4, SAS Institute, Cary, NC) according to a two-factor (component and treatment time) linear model. The assumptions of normal distribution and homogeneity of variance were tested and the variance grouping technique was used to correct for variance heterogeneity. Sidak adjusted p-values were used to maintain experiment-wise error ≤ 0.05. The ethylene adsorption isotherm and release from Al-MOF@alginate-Fe(III) beads were carried out in duplicate. Data are reported as the mean ± standard error (SE). The analysis of variance (ANOVA) with the Duncan method followed by multiple post hoc comparisons were carried out to determine any significant differences ($p < 0.05$) using the Statistical Product and Service Solutions (SPSS) 16.0 software (SPSS Inc., Chicago, IL, USA).

3. Results and discussion

3.1. Al-MOF properties

The hydrothermally synthesized Al-MOF powders exhibited a hexagonal crystal structure (Fig. 1a) as observed under a polarizing microscope. A significant electron diffraction pattern of Al-MOF powder was further revealed using TEM (Fig. 1b), indicating significant crystallinity. The SEM-EDS analysis showed that the fabricated Al-MOF powder exhibited uniform distribution of elements Al, C and O (Fig. 1c). All these characterizations indicate that the Al, C, and O atoms were evenly distributed in the structure of Al-MOF crystals.

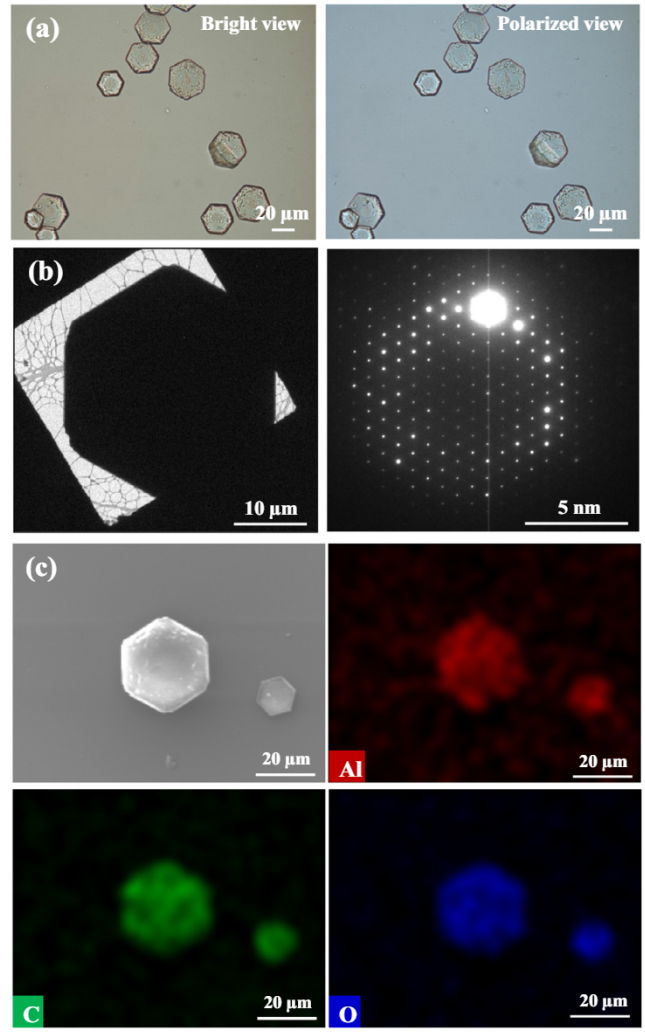

Fig. 1. (a) The Al-MOF crystal structure observed using a polarizing microscope with bright and polarized views. (b) TEM observation of the Al-MOF powder and electron diffraction pattern show a significant crystallinity. And (c) SEM-EDS images of the Al-MOF crystals show an even distribution of the elements Al, C and O.

The hydrothermal method with self-formed vapor pressure is a powerful means to fabricate MOF crystals [43,45–47]. Both temperature and pressure are important for providing bonding energy in seed crystal synthesis and growth in the solid phase [48]. The aluminous-nodal MOFs synthesized by the hydrothermal method such as MIL96 and MIL100 were stable in air and aqueous media [43,49]. Therefore, these MOFs are suitable for further encapsulation in a water-based environment. In the present study, the sealed autoclave reactors with Teflon liners created a high-pressure aqueous vapor-filled environment, which provided bonding energy for Al-MOF seed crystal synthesis and growth [2,48]. Moreover, the HF and TEOS added at the beginning of the Al-MOF synthetic reaction at concentrations of 0.14 and 0.8% w/w resulted in a mineralizing effect under hydrothermal conditions, which increased Al-MOF crystallinity. HF and TEOS did not leave residuel in the final products [43] and therefore do not affect the safety.

The XRD analysis of Al-MOF powder was performed to verify the crystal structure and properties. As shown in Fig. 2, the experimental XRD pattern was exactly matched with the calculated pattern of Al-MOF from the CCDC database. The three crystallographic sites of Al were connected with ligands $[btc]^{3-}$ (Fig. 3a), forming a

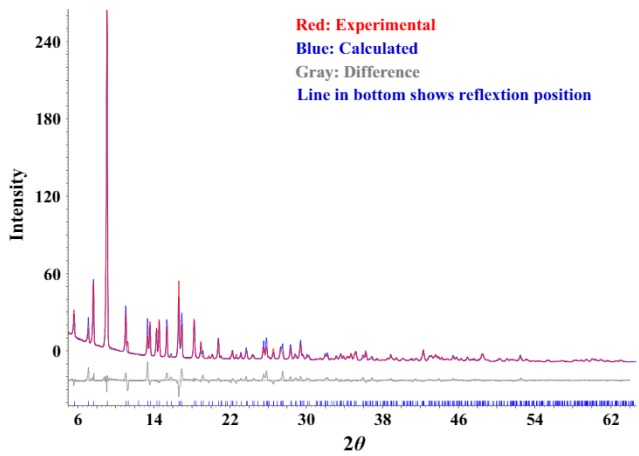

Fig. 2. Comparison of XRD patterns for the laboratory produced Al-MOF powders and identified crystal diffraction pattern for Al-MOF from the ICDD database.

hexagonal ($P6_3/mmc$) unit cell of dimensions $14.28 \times 14.28 \times 31.32$ Å^3 with detailed crystal information shown in the Table S1, and growing to a 3D framework (Fig. 3b and c).

3.2. Ethylene sorption capability

The sorption isotherm at 25 °C shows a kinetic absorption of ethylene by 20 mg of Al-MOF crystals at pressures of 0–101.3 kPa (Fig. 4). The isotherm was fitted to a linear model, suggesting a constant sorption rate of ethylene at different pressures below 101.3 kPa. The determined ethylene absorption efficiency was 41.0 cm^3/g at standard atmospheric conditions (temperature of 25 °C and pressure of 101.3 kPa), which was close to the reported absorption efficiency of 42.0 cm^3/g by the MIL-101 [50].

The result of ethylene sorption isotherm highlighted a possible relative electronegativity of the benzene ligand of Al-MOF crystals, which engenders interaction with the π bonds of ethylene [51]. Additionally, the presence of the unsaturated aluminum ion sites for coordination bonding with ligands have a greater ionic valence, resulting in stronger adsorbate-metal interactions with ethylene [52]. The ethylene sorption by MOFs depends on the interfacial pore volume and specific surface area, unsaturated metal ion sites, and ligand chemical structure. The interfacial pore volume and specific surface area provide physical channels for ethylene absorption into MOFs; meanwhile, the unsaturated metal ion sites and ligands provide binding sites for ethylene adsorption in MOFs. The ethylene uptake is a critical parameter to evaluate the MOF. This is determined by the structure of MOF, as well as its interaction with ethylene. An elaborate comparison on gas absorption properties by various MOFs was listed in Tables S2 and S3 in the Supporting Information.

We also attempted to test the porosity of Al-MOF by nitrogen sorption. Interestingly, no absorption of nitrogen by the fabricated Al-MOF crystals was detected at 77 K (Fig. S1). This may be caused by contractible interfacial pore size of Al-MOF, which was also reported by a previous study, and probably caused by the unsuitable temperature [43]. The contractible interfacial pore size at 77 K is likely attributed to the temperature induced layer-elastic structure of layer-structured MOFs [53].

Besides ethylene uptake, other factors including safety and solvent compatibility are also crucial for specific applications in practice. For instance, household fruit ripening does not require high concentration of ethylene, but safety, continuous release, and compatibility with water (or food-grade salt aqueous solutions) are imperative. Therefore, Al-MOF as a safe formula (neither metal ions nor ligands is potentially toxic) is an ideal core material for this type of applications.

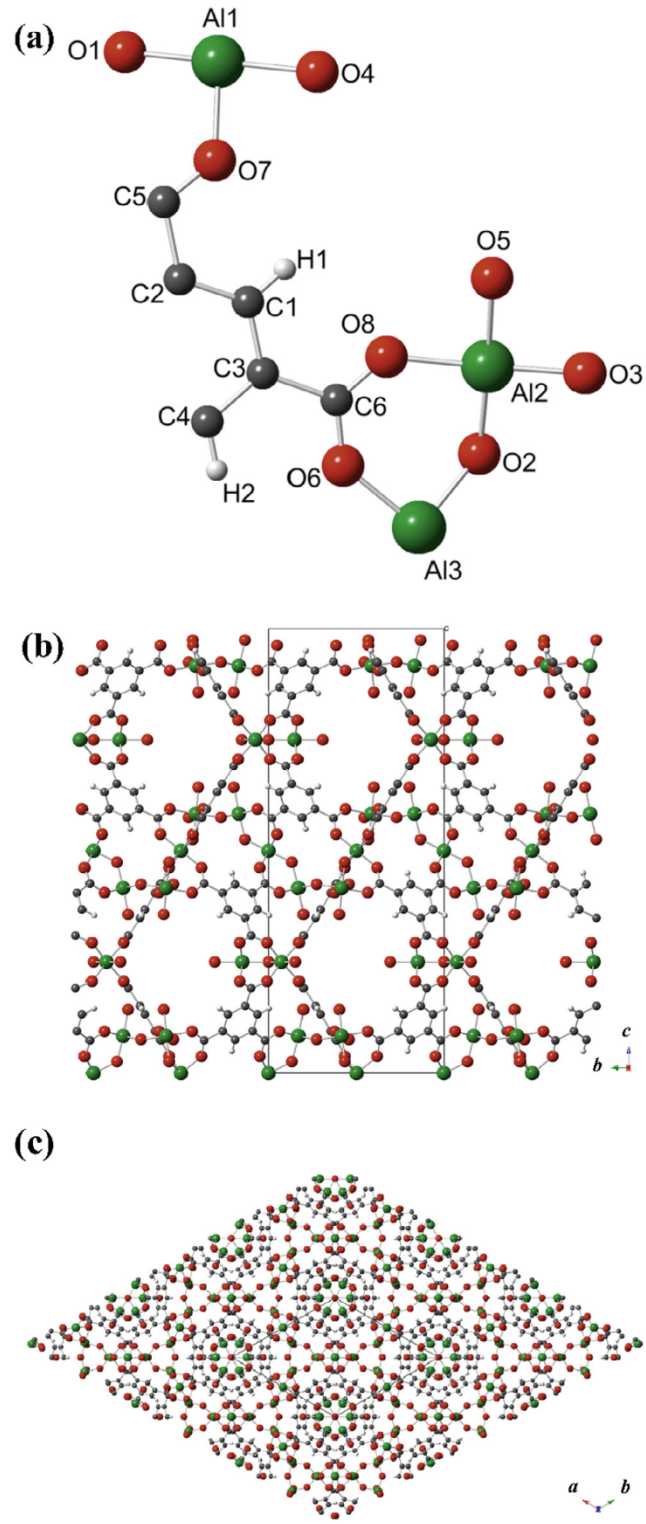

Fig. 3. (a) Molecular structure of the Al-MOF, (b) view along the *a* axis of the Al-MOF unit cell to *b*-*c* surface, and (c) view along the *c* axis of the Al-MOF unit cell to *a*-*b* surface.

3.3. Al-MOF@alginate-Fe(III) composite properties

The SEM images of the cross section of dried Al-MOF@alginate-Fe(III) bead was shown in Fig. 5. The embedded Al-MOF crystals

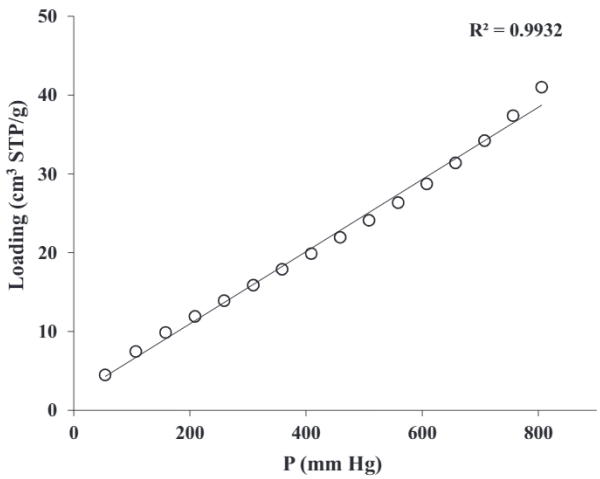

Fig. 4. Ethylene sorption isotherm by Al-MOF at low pressures (P < 101.3 kPa) and 25 °C.

were clearly observed on the cross section of the Al-MOF@alginate-Fe(III) bead. The alginate-Fe(III) bead (Control) cross section showed a smooth structure. Additionally, the SEM-EDS revealed the different distribution of Al, C, O and Fe on the cross section and surface of Al-MOF@alginate-Fe(III) bead (Fig. 6a). Clearly, Al signal intensity was significantly higher on the cross section of Al-MOF@alginate-Fe(III) bead than on the surface. Meanwhile, the C, O and Fe signal intensity showed no significant differences (Fig. 6b). These results indicate that the Al-MOF crystals were mainly entrapped inside the Fe(III)-solidified alginate matrix. The tightly entrapped Al-MOF crystals loaded in alginate-Fe(III) composites is expected to decrease the exposure of Al-MOF crystal interfacial pores. In addition, the mass differential analysis showed that the Al-MOF@alginate-Fe(III) beads contained 46.7% Al-MOF crystals and 7.4% Fe (Fig. 7).

The dynamic release of Al-MOF and Fe from Al-MOF@alginate-Fe(III) beads was shown in Fig. 8. It is clear that the MOF component was almost completely released from the matrix after 2.5-h immersion in 200 mM NaCit solution. These results suggested that the NaCit solution is a potential promoter for the exposure of embedded Al-MOF and the degradation of alginate-Fe(III) matrix, and consequently, the release of ethylene entrapped within Al-MOF interfacial pores.

The cross-linking of alginate molecules with iron ions by coordinate bonds has been demonstrated to form a stable egg-box structure [30], similar to that reported for the calcium and ion-alginate complex [31]. The generated egg-box structure formed a close-knit carrier to load Al-MOF crystals after drying, as observed via the SEM. Additionally, the elemental distribution analysis by EDS demonstrated that the Al-MOF crystals were primarily packaged in the interior of the alginate-Fe(III) beads, which would further prevent the release of volatile ethylene. Dynamic degradation of Al-MOF@alginate-Fe(III) beads led to the similar release rates in both Al-MOF crystals and iron ions from the Al-MOF@alginate-Fe(III) beads in 200 mM NaCit solution. It is suggested that the dissociation of iron ions from alginate-Fe(III) matrix, followed by bead degradation, proceeded simultaneously with the release of entrapped Al-MOF crystals. The degradation of the matrix was possibly driven by two factors, i.e., pore swelling upon water absorption, and replacement of iron by sodium, due to the chelation effect of citrate on iron ions [30]. Additionally, similar degradation effects of alginate-Fe(III) composites to expose Al-MOF crystals were found in 400 mM NaCit solution (data not shown) as in 200 mM NaCit solution (Fig. 8) in our preliminary experiment. Hence, in the present case, the 200 mM NaCit solution was used as a high-efficiency "promoter" to expose packaged Al-MOF crystals for further controlled release of ethylene from the Al-MOF crystal interfacial pores.

3.4. Dynamic release of ethylene

The controlled release of ethylene is important for practical applications. As shown in Fig. 9, ethylene was released gradually during the 3-h kinetic releasing test. When immersed in 200 mM NaCit solution, the Al-MOF@alginate-Fe(III) beads released 8.2–9.1 mg/L (i.e., 0.41–0.46 mg/L per mg Al-MOF) ethylene in a 4-L glass jar, compared to 2.6–4.0 mg/L (i.e., 0.13–0.20 mg/L per

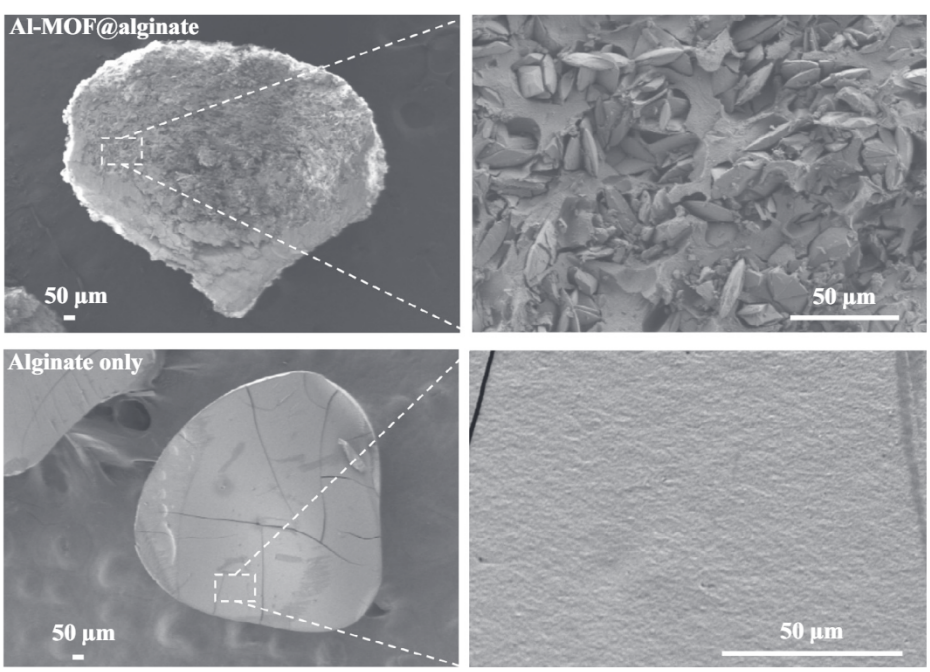

Fig. 5. SEM images of the cross section of dried Al-MOF@alginate-Fe(III) bead (top) and alginate-Fe(III) bead (bottom).

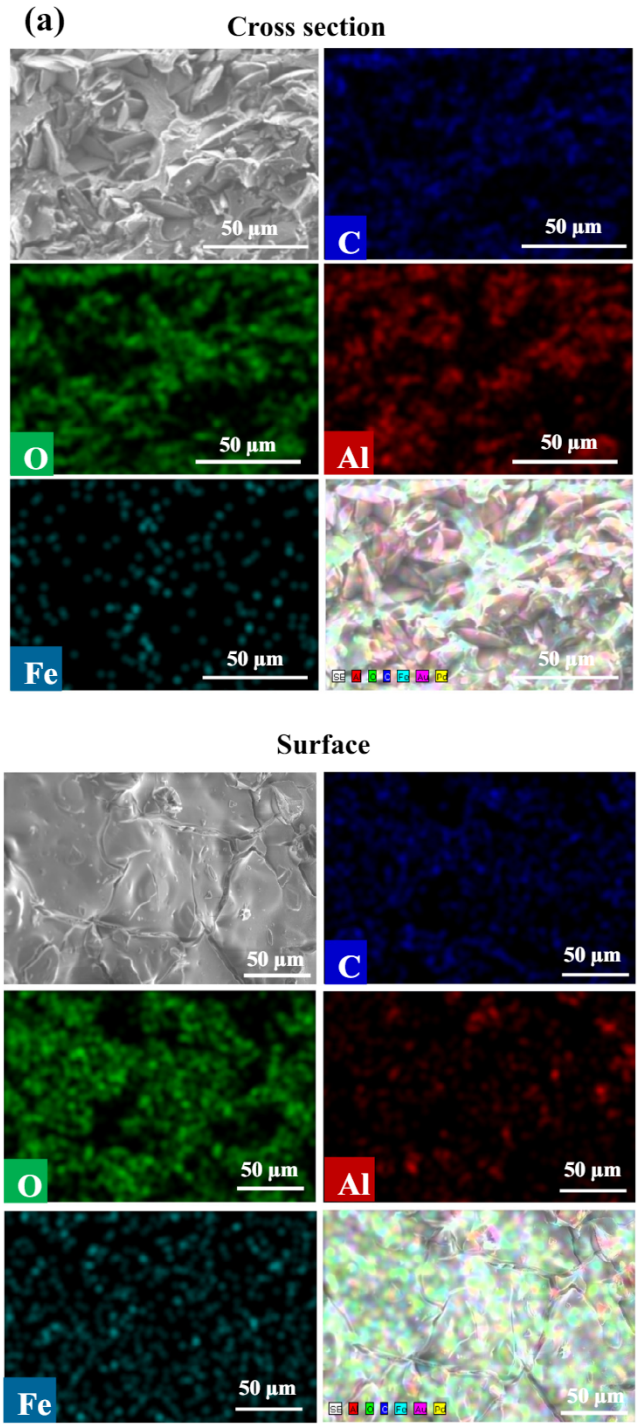

Fig. 6. The SEM-EDS analysis of the cross section and surface of the Al-MOF@alginate-Fe(III) bead. (a) The element distribution map of Al, C, O and Fe, and SEM observation of cross section and surface of the Al-MOF@alginate-Fe(III) bead. (b) The elementary signal intensity of C, O, Fe, Al, and Cl on the cross section and surface of the Al-MOF@alginate-Fe(III) bead.

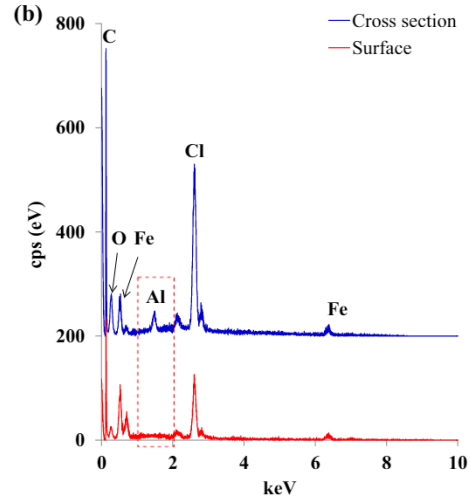

Fig. 6 (*continued*)

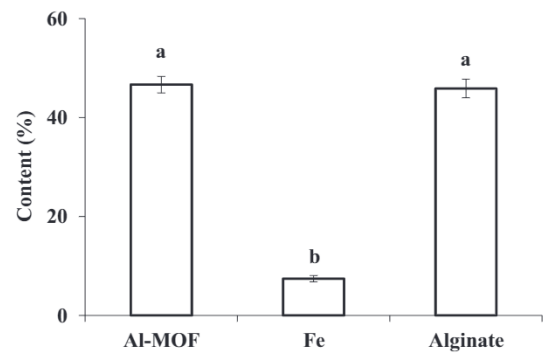

Fig. 7. The bright images of Al-MOF@alginate-Fe(III) beads before and after drying, and the contents of Al-MOF, Fe, and alginate in the dried Al-MOF@alginate-Fe(III) beads.

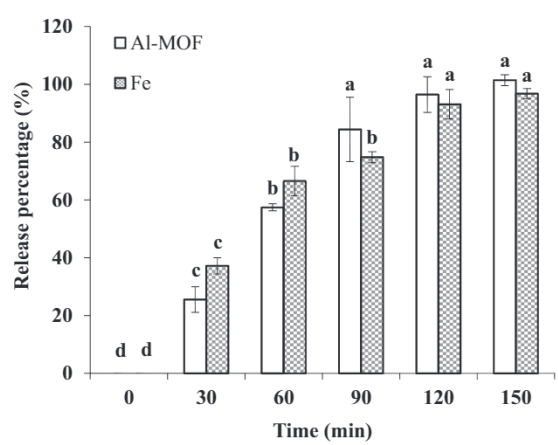

Fig. 8. The dynamic release of Al-MOF and Fe from Al-MOF@alginate-Fe(III) beads in 200 mM NaCit solution without pH adjustment. Different lower case letters indicate significant differences in release percentages at different exposure times for each component. There were no significant differences in release percentages between the two components. Error bars show the standard error of the mean for 3 replicate batches of Al-MOF production.

mg Al-MOF) when they were immersed in water. Matrix degradation aided by NaCit was probably the driving force for ethylene release as discussed in the previous paragraph. The alginate-Fe(III) beads without the Al-MOF crystals were also charged with ethylene and treated with 200 mM NaCit solution. No ethylene release was detected from alginate-Fe(III) beads, indicating that these alginate-Fe(III) composites alone cannot absorb ethylene by their own. No significant increase of ethylene concentration in air at ambient temperature and pressure was found within 3 h, suggesting possible saturation of ethylene in the container. Similar results were found in our previous research using a copper

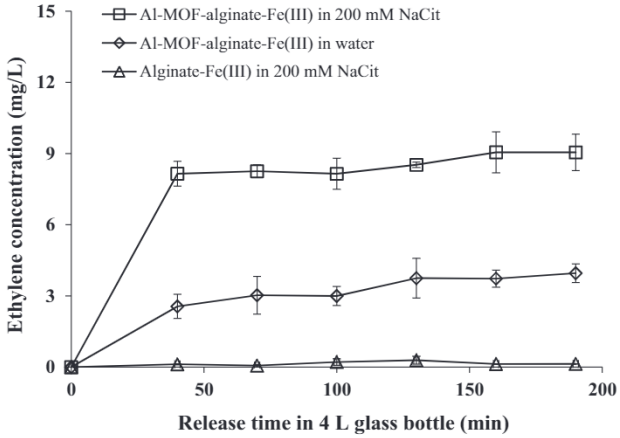

Fig. 9. The kinetics of ethylene release from 43 mg of dried ethylene loaded Al-MOF@alginate-Fe(III) beads in 10 mL of 200 mM NaCit and water in a 4 L container. The same mass of dried alginate-Fe(III) beads were dispersed in 10 mL of 200 mM NaCit as control. No repeat experiments was carried out on the ethylene concentration released from alginate-Fe(III) in 200 mM NaCit (triangle) at 160 and 190 min only because of equipment failure. Other data are duplicate repetition.

terephthalate MOF (CuTPA) [2]. Based on our results, the Al-MOF@alginate-Fe(III) bead is a potential candidate for the practical applications of ethylene storage and controlled release. For example, it may be applied in fruit ripening, where ethylene is preferably stored under ambient conditions prior to use and then released at low concentrations (typically several miligrams per liter) when the package is triggered on.

4. Conclusions

In the present study, we developed a novel solid Al-MOF@alginate-Fe(III) matrix for ethylene storage and controlled release using 200 mM NaCit solution as a promoter. The hexagonal ($P6_3/mmc$) Al-MOF crystals were successfully embedded in an alginate-Fe(III) matrix comprising 46.7% Al-MOF and 7.4% Fe(III). This Al-MOF@alginate-Fe(III) matrix dissociated effectively within 2.5 h when immersed in 200 mM NaCit solution. The matrix degradation accounted for nearly complete release of the Al-MOF crystals, followed by the release of entrapped ethylene at 0.41–0.46 mg/L per mg Al-MOF in a 4-L glass jar within 3 h. The ability to degrade the ethylene storage matrix on demand by exposure to NaCit provides a potential encapsulation system which may enable practical applications, such as consumer or retail use for climacteric fruit ripening at the point of sale or consumption [2]. This may reduce post-harvest loss and waste of tropical or subtropic fruits assocaited with over ripening occured after ethylene treatment and before consumption.

Acknowledgements

The authors wish to thank Ellen Turner for proof reading the manuscript and strong technical support in statistical analysis. The authors also wish to thank Dr. Bin Zhou for his outstanding contribution of the instrument debugging for this study. This research was supported by USDA-National Institute of Food and Agriculture Specialty Crops Research Initiative (Award No. 2016-51181-25403), USDA-ARS (Project No. 1275-43440-006-00D), and USDA-NIFA (Award No. 2016-10382 and 2014-67021-21585). Mention of trade names or commercial products in this publication is solely for the purpose of providing specific information and does not imply recommendation or endorsement by the USDA.

Appendix A. Supplementary material

Supplementary data associated with this article can be found, in the online version, at https://doi.org/10.1016/j.jcis.2018.08.057.

References

[1] H. Furukawa, O. Yaghi, Storage of hydrogen, methane, and carbon dioxide in highly porous covalent organic frameworks for clean energy applications, J. Am. Chem. Soc. 131 (25) (2009) 8875–8883.
[2] B. Zhang, Y. Luo, K. Kanyuck, G. Bauchan, J. Mowery, P. Zavalij, Development of metal-organic framework for gaseous plant hormone encapsulation to manage ripening of climacteric produce, J. Agric. Food. Chem. 64 (25) (2016) 5164–5170.
[3] D. Zheng, L. Wang, T. Yang, Y. Zhang, Q. Wang, M. Kurmoo, M. Zeng, A porous metal organic framework [Zn_2(bdc)(L-lac)] as a coating material for capillary columns of gas chromatography, Inorg. Chem. 56 (18) (2017) 11043–11049.
[4] X. Cui, K. Chen, H. Xing, Q. Yang, R. Krishna, Z. Bao, H. Wu, W. Zhou, X. Dong, Y. Han, B. Li, Q. Ren, M. Zaworotko, B. Chen, Pore chemistry and size control in hybrid porous materials for acetylene capture from ethylene, Science 353 (6295) (2016) 141–144.
[5] J. Rowsell, O. Yaghi, Strategies for hydrogen storage in metal-organic frameworks, Angew. Chem. Int. Edit. 44 (30) (2005) 4670–4679.
[6] J. Mason, J. Oktawiec, M. Taylor, M. Hudson, J. Rodriguez, J. Bachman, M. Gonzalez, A. Cervellino, A. Guagliardi, C. Brown, P. Llewellyn, N. Masciocchi, J. Long, Methane storage in flexible metal-organic frameworks with intrinsic thermal management, Nature 527 (7578) (2015) 357.
[7] M. Andres, M. Benzaqui, C. Serre, N. Steunou, I. Gascon, Fabrication of ultrathin MIL-96(Al) films and study of CO_2 adsorption/desorption processes using quartz crystal microbalance, J. Colloid Interf. Sci. 519 (2018) 88–96.
[8] M. Mayer, D. Dedovets, Y. Guari, J. Larionova, J. Long, J. Causse, Synthesis of poly(diallyldimethylammonium) capped copper hexacyanoferrate (CuHCF) nanoparticles: an efficient stabiliser for pickering emulsions, J. Colloid Interf. Sci. 505 (2017) 364–372.
[9] H. Deng, S. Grunder, K. Cordova, C. Valente, H. Furukawa, M. Hmadeh, F. Gandara, A. Whalley, Z. Liu, S. Asahina, H. Kazumori, M. O'Keeffe, O. Terasaki, J. Stoddart, O. Yaghi, Large-pore apertures in a series of metal-organic frameworks, Science 336 (6084) (2012) 1018–1023.
[10] J. Duan, M. Higuchi, J. Zheng, S. Noro, I. Chang, K. Hyeon-Deuk, S. Mathew, S. Kusaka, E. Sivaniah, R. Matsuda, S. Sakaki, S. Kitagawa, Density gradation of open metal sites in the mesospace of porous coordination polymers, J. Am. Chem. Soc. 139 (33) (2017) 11576–11583.
[11] A. Nelson, O. Farha, K. Mulfort, J. Hupp, Supercritical processing as a route to high internal surface areas and permanent microporosity in metal-organic framework materials, J. Am. Chem. Soc. 131 (2) (2009) 458–460.
[12] L. Ma, J. Falkowski, C. Abney, W. Lin, A series of isoreticular chiral metal-organic frameworks as a tunable platform for asymmetric catalysis, Nat. Chem. 2 (10) (2010) 838–846.
[13] G. Lu, S. Li, Z. Guo, O. Farha, B. Hauser, X. Qi, Y. Wang, X. Wang, S. Han, X. Liu, J. DuChene, H. Zhang, Q. Zhang, X. Chen, J. Ma, S. Loo, W. Wei, Y. Yang, J. Hupp, F. Huo, Imparting functionality to a metal-organic framework material by controlled nanoparticle encapsulation, Nat. Chem. 4 (4) (2012) 310–316.
[14] K. Sumida, D. Rogow, J. Mason, T. McDonald, E. Bloch, Z. Herm, T. Bae, J. Long, Carbon dioxide capture in metal-organic frameworks, Chem. Rev. 112 (2) (2012) 724–781.
[15] D. Alezi, Y. Belmabkhout, M. Suyetin, P. Bhatt, L. Weselinski, V. Solovyeva, K. Adil, I. Spanopoulos, P. Trikalitis, A. Emwas, M. Eddaoudi, MOF crystal chemistry paving the way to gas storage needs: aluminum-based soc-MOF for CH_4, O_2, and CO_2 storage, J. Am. Chem. Soc. 137 (41) (2015) 13308–13318.
[16] M. Azhar, H. Abid, V. Periasamy, H. Sun, M. Tade, S. Wang, Adsorptive removal of antibiotic sulfonamide by UiO-66 and ZIF-67 for wastewater treatment, J. Colloid Interf. Sci. 500 (2017) 88–95.
[17] A. Corma, H. Garcia, F. Xamena, Engineering metal organic frameworks for heterogeneous catalysis, Chem. Rev. 110 (8) (2010) 4606–4655.
[18] M. Hu, V. Safarifard, E. Doustkhah, S. Rostamnia, A. Morsali, N. Nouruzi, S. Beheshti, K. Akhbari, Taking organic reactions over metal-organic frameworks as heterogeneous catalysis, Micropor. Mesopor. Mat. 256 (2018) 111–127.
[19] S. Rostamnia, H. Alamgholiloo, X. Liu, Pd-grafted open metal site copper-benzene-1,4-dicarboxylate metal organic frameworks (Cu-BDC MOF's) as promising interfacial catalysts for sustainable Suzuki coupling, J. Colloid Interf. Sci. 469 (2016) 310–317.
[20] S.R. Hassan Alamgholiloo, Asadollah Hassankhani, Reza Banaei, Synthesis of a zeolitic imidazolate-zinc metal-organic framework and the combination of its catalytic properties with 2,2,2-trifluoroethanol for N-formylation, Synlett 29 (12) (2018) 1593–1596.
[21] S. Rostamnia, F. Mohsenzad, Nanoarchitecturing of open metal site Cr-MOFs for oxodiperoxo molybdenum complexes [$MoO(O_2)_2$@En/MIL-100(Cr)] as promising and bifunctional catalyst for selective thioether oxidation, Mol. Catal. 445 (2018) 12–20.
[22] P. Freund, I. Senkovska, S. Kaskel, Switchable conductive MOF-nanocarbon composite coatings as threshold sensing architectures, ACS Appl. Mater. Int. 9 (50) (2017) 43782–43789.

[23] S. Yuan, L. Zou, H. Li, Y. Chen, J. Qin, Q. Zhang, W. Lu, M. Hall, H. Zhou, Flexible zirconium metal-organic frameworks as bioinspired switchable catalysts, Angew. Chem. Int. Ed. 55 (36) (2016) 10776–10780.
[24] H. Li, H. Xu, S. Zang, T. Mak, A viologen-functionalized chiral Eu-MOF as a platform for multifunctional switchable material, Chem. Commun. 52 (3) (2016) 525–528.
[25] J. Park, D. Yuan, K. Pham, J. Li, A. Yakovenko, H. Zhou, Reversible alteration of CO_2 adsorption upon photochemical or thermal treatment in a metal-organic framework, J. Am. Chem. Soc. 134 (1) (2012) 99–102.
[26] L. Li, Y. Fang, R. Vreeker, I. Appelqvist, E. Mendes, Reexamining the egg-box model in calcium-alginate gels with X-ray diffraction, Biomacromolecules 8 (2) (2007) 464–468.
[27] P. Sikorski, F. Mo, G. Skjak-Braek, B. Stokke, Evidence for egg-box-compatible interactions in calcium-alginate gels from fiber X-ray diffraction, Biomacromolecules 8 (7) (2007) 2098–2103.
[28] A. Decho, Imaging an alginate polymer gel matrix using atomic force microscopy, Carbohyd. Res. 315 (3–4) (1999) 330–333.
[29] D. Li, C. Lv, L. Liu, Y. Xia, X. She, S. Guo, D. Yang, Egg-box structure in cobalt alginate: a new approach to multifunctional hierarchical mesoporous N-doped carbon nanofibers for efficient catalysis and energy storage, ACS Central Sci. 1 (5) (2015) 261–269.
[30] R. Narayanan, G. Melman, N. Letourneau, N. Mendelson, A. Melman, Photodegradable iron(III) cross-linked alginate gels, Biomacromolecules 13 (8) (2012) 2465–2471.
[31] Y. Murata, Y. Kodama, T. Isobe, K. Kofuji, S. Kawashima, Drug release profile from calcium-induced alginate-phosphate composite gel beads, Int. J. Polym. Sci. 2009 (2009) 729057.
[32] P. Vennestrom, C. Osmundsen, C. Christensen, E. Taarning, Beyond petrochemicals: the renewable chemicals industry, Angew. Chem. Int. Ed. 50 (45) (2011) 10502–10509.
[33] P. Anastas, N. Eghbali, green chemistry: principles and practice, Chem. Soc. Rev. 39 (1) (2010) 301–312.
[34] F. Roberts, K. Kuhl, A. Nilsson, High selectivity for ethylene from carbon dioxide reduction over copper nanocube electrocatalysts, Angew. Chem. Int. Ed. 54 (17) (2015) 5179–5182.
[35] N. Patel, A. Whitehead, J. Newman, M. Caldorera-Moore, Poly(ethylene glycol) hydrogels with tailorable surface and mechanical properties for tissue engineering applications, ACS Biomater. – Sci. Eng. 3 (8) (2017) 1494–1498.
[36] M. Liu, B. Gomes, I. Mila, E. Purgatto, L. Peres, P. Frasse, E. Maza, M. Zouine, J. Roustan, M. Bouzayen, J. Pirrello, Comprehensive profiling of ethylene response factor expression identifies ripening-associated ERF genes and their link to key regulators of fruit ripening in tomato, Plant Physiol. 170 (3) (2016) 1732–1744.
[37] K. Kazan, Diverse roles of jasmonates and ethylene in abiotic stress tolerance, Trends Plant Sci. 20 (4) (2015) 219–229.
[38] K. Shibasaki, A. Fujii, N. Mikami, S. Tsuzuki, Magnitude and nature of interactions in benzene-X (X = ethylene and acetylene) in the gas phase: significantly different CH/pi interaction of acetylene as compared with those of ethylene and methane, J. Phys. Chem. A 111 (5) (2007) 753–758.
[39] J. Canivet, S. Aguado, Y. Schuurman, D. Farrusseng, MOF-supported selective ethylene dimerization single-site catalysts through one-pot postsynthetic modification, J. Am. Chem. Soc. 135 (11) (2013) 4195–4198.
[40] S. Xiang, Z. Zhang, C. Zhao, K. Hong, X. Zhao, D. Ding, M. Xie, C. Wu, M. Das, R. Gill, K. Thomas, B. Chen, Rationally tuned micropores within enantiopure metal-organic frameworks for highly selective separation of acetylene and ethylene, Nat. Commun. 2 (2011) 204.
[41] S. Madrahimov, J. Gallagher, G. Zhang, Z. Meinhart, S. Garibay, M. Delferro, J. Miller, O. Farha, J. Hupp, S. Nguyen, Gas-phase dimerization of ethylene under mild conditions catalyzed by MOF materials containing (bpy)Ni-II complexes, ACS Catal. 5 (11) (2015) 6713–6718.
[42] T. Hu, H. Wang, B. Li, R. Krishna, H. Wu, W. Zhou, Y. Zhao, Y. Han, X. Wang, W. Zhu, Z. Yao, S. Xiang, B. Chen, Microporous metal-organic framework with dual functionalities for highly efficient removal of acetylene from ethylene/acetylene mixtures, Nat. Commun. 6 (2015) 7328.
[43] T. Loiseau, L. Lecroq, C. Volkringer, J. Marrot, G. Ferey, M. Haouas, F. Taulelle, S. Bourrelly, P. Llewellyn, M. Latroche, MIL-96, a porous aluminum trimesate 3D structure constructed from a hexagonal network of 18-membered rings and mu(3)-oxo-centered trinuclear units, J. Am. Chem. Soc. 128 (31) (2006) 10223–10230.
[44] W. Zhou, Robert Apkarian, Zhong Lin Wang, David Joy, Fundamentals of Scanning Electron Microscopy (SEM), Scanning Microscopy for Nanotechnology, Springer, New York, 2006, pp. 1–40.
[45] G. Wang, Y. Lei, N. Wang, R. He, H. Jia, N. Hu, J. Xu, Construction of metal-organic frameworks with tetranuclear metal clusters: hydrothermal synthesis, structure, and magnetic properties, Cryst. Growth Des. 10 (2) (2010) 534–540.
[46] R. Pena-Rodriguez, E. Marquez-Lopez, A. Guerrero, L. Chinas, D. Hernandez-Gonzalez, J. Rivera, Hydrothermal synthesis of cobalt (II) 3D metal-organic framework acid catalyst applied in the transesterification process of vegetable oil, Mater. Lett. 217 (2018) 117–119.
[47] M. Haouas, C. Volkringer, T. Loiseau, G. Ferey, F. Taulelle, In situ NMR, ex situ XRD and SEM study of the hydrothermal crystallization of nanoporous aluminum trimesates MIL-96, MIL-100, and MIL-110, Chem. Mater. 24 (13) (2012) 2462–2471.
[48] J. Karpinski, S. Kazakov, J. Jun, M. Angst, R. Puzniak, A. Wisniewski, P. Bordet, Single crystal growth of MgB_2 and thermodynamics of Mg-B-N system at high pressure, Physica C 385 (1–2) (2003) 42–48.
[49] C. Volkringer, D. Popov, T. Loiseau, G. Ferey, M. Burghammer, C. Riekel, M. Haouas, F. Taulclle, Synthesis, single-crystal X-ray microdiffraction, and NMR characterizations of the giant pore metal-organic framework aluminum trimesate MIL-100, Chem. Mater. 21 (24) (2009) 5695–5697.
[50] Y. Zhang, B. Li, R. Krishna, Z. Wu, D. Ma, Z. Shi, T. Pham, K. Forrest, B. Space, S. Ma, Highly selective adsorption of ethylene over ethane in a MOF featuring the combination of open metal site and pi-complexation, Chem. Commun. 51 (13) (2015) 2714–2717.
[51] J. Novoa, F. Mota, The C-H center dot center dot center dot pi bonds: strength, identification, and hydrogen-bonded nature: a theoretical study, Chem. Phys. Lett. 318 (4–5) (2000) 345–354.
[52] Z. Bao, L. Yu, Q. Ren, X. Lu, S. Deng, Adsorption of CO_2 and CH_4 on a magnesium-based metal organic framework, J. Colloid Interf. Sci. 353 (2) (2011) 549–556.
[53] H. Kanoh, A. Kondo, H. Noguchi, H. Kajiro, A. Tohdoh, Y. Hattori, W. Xu, M. Moue, T. Sugiura, K. Morita, H. Tanaka, T. Ohba, K. Kaneko, Elastic layer-structured metal organic frameworks (ELMS), J. Colloid Interf. Sci. 334 (1) (2009) 1–7.